Cellular and Molecular Life Sciences (2023) 80:223
https://doi.org/10.1007/s00018-023-04866-w



ORIGINAL ARTICLE

# Kindlin-2 controls angiogenesis through modulating Notch1 signaling

Yuechao Dong[1] · Guixing Ma[1] · Xiaoting Hou[1] · Yingying Han[1] · Zhen Ding[1] · Wanze Tang[1] · Litong Chen[1] · Yangshan Chen[1] · Bo Zhou[1] · Feng Rao[2] · Kaosheng Lv[1] · Changzheng Du[1] · Huiling Cao[1]

Received: 22 March 2023 / Revised: 2 July 2023 / Accepted: 8 July 2023 / Published online: 22 July 2023


## Abstract

Kindlin-2 is critical for development and homeostasis of key organs, including skeleton, liver, islet, etc., yet its role in modulating angiogenesis is unknown. Here, we report that sufficient KINDLIN-2 is extremely important for NOTCH-mediated physiological angiogenesis. The expression of KINDLIN-2 in HUVECs is significantly modulated by angiogenic factors such as vascular endothelial growth factor A or tumor necrosis factor α. A strong co-localization of CD31 and Kindlin-2 in tissue sections is demonstrated by immunofluorescence staining. Endothelial-cell-specific Kindlin-2 deletion embryos die on E10.5 due to hemorrhage caused by the impaired physiological angiogenesis. Experiments in vitro show that vascular endothelial growth factor A-induced multiple functions of endothelial cells, including migration, matrix proteolysis, morphogenesis and sprouting, are all strengthened by KINDLIN-2 overexpression and severely impaired in the absence of KINDLIN-2. Mechanistically, we demonstrate that KINDLIN-2 inhibits the release of Notch intracellular domain through binding to and maintaining the integrity of NOTCH1. The impaired angiogenesis and avascular retinas caused by KINDLIN-2 deficiency can be rescued by DAPT, an inhibitor of γ-secretase which releases the intracellular domain from NOTCH1. Moreover, we demonstrate that high glucose stimulated hyperactive angiogenesis by increasing KINDLIN-2 expression could be prevented by KINDLIN-2 knockdown, indicating Kindlin-2 as a potential therapeutic target in treatment of diabetic retinopathy. Our study for the first time demonstrates the significance of Kindlin-2 in determining Notch-mediated angiogenesis during development and highlights Kindlin-2 as the potential therapeutic target in angiogenic diseases, such as diabetic retinopathy.

**Keywords** Endothelial Kindlin-2 · Angiogenesis · Notch1 · NICD

## Abbreviations

| | |
|---|---|
| VEGFA | Vascular endothelial growth factor A |
| VEGFR2 | Vascular endothelial growth factor receptor 2 |
| NICD | Notch intracellular domain |
| DAPT | *N*-[*N*-(3,5-Difluorophenacetyl-L-alanyl)]-*S*-phenylglycine *t*-butyl ester |
| Hg | High glucose |
| Ng | Normal glucose |
| NC | Negative control |
| ECs | Endothelial cells |
| HUVECs | Human umbilical vascular ECs |
| DR | Diabetic retinopathy |
| BM | Basement membrane |
| MMP | Matrix metalloprotease |
| RBP-Jκ | Recombination signal-binding protein Jκ |
| Dll4 | Delta-like 4 |
| FERM | Four-point-one, ezrin, radixin, moesin |
| TNFα | Tumor necrosis factor α |
| PECAM-1 | Platelet endothelial cell adhesion molecule 1 |
| CD31 | Cluster of differentiation 31 |
| CKO | Conditional knockout |
| IHC | Immunohistochemistry |
| IF | Immunofluorescence |
| WB | Western blotting |

Yuechao Dong, Guixing Ma, Xiaoting Hou and Yingying Han contributed equally to this study.

✉ Guixing Ma
maguixing@live.com

✉ Huiling Cao
caohl@sustech.edu.cn

[1] Department of Biochemistry, School of Medicine, Southern University of Science and Technology, Guangdong Provincial Key Laboratory of Cell Microenvironment and Disease Research, Key University Laboratory of Metabolism and Health of Guangdong, Southern University of Science and Technology, Shenzhen 518055, China

[2] Southern University of Science and Technology, Shenzhen 518055, China

| | |
|---|---|
| AIA | Angiogenesis invasion assay |
| QRT-PCR | Quantitative real time-polymerase chain reaction |
| IP | Immunoprecipitation |
| CHX | Cycloheximide |
| HIF-1α | Hypoxia inducible factor-1α |
| EdU | 5-Ethynyl-29-deoxyuridine |
| SiRNA | Small interfering RNA |

## Introduction

Angiogenesis is the sprouting of activated endothelial cells (ECs) from the pre-existing vasculature to generate neo-vessels, which is essential for embryonic development, tissue reproduction and repair [1, 2]. Mechanically, the pro-angiogenic factor vascular endothelial growth factor A (VEGFA) activates vascular endothelial growth factor receptor type 2 (VEGFR2) of ECs and induces their subsequent activities. It is well demonstrated in previous studies that VEGF-induced sprouting, migration, and tube formation competences of ECs [3]. Angiogenesis requires the cooperation between tip cells and stalk cells, and the two adjacent and functional ECs are coordinated by Notch1 signal. In tip cells equipped with elongated filopodias, VEGFR2 phosphorylation increases Notch ligand Delta-like 4 (Dll4), which mediates the activation of Notch1 signal to suppress tip cell phenotype in the neighboring stalk cells. In contrast, excessive sprouting results from the inhibition of Dll4-Notch1 interaction [4].

Physiological angiogenesis responsible for development requires the balance of pro-angiogenic factors and anti-angiogenic factors. Disturbance of the balance induces pathological angiogenesis characterized by endothelial overgrowth, thinner and more permeable vascular walls. Consequently, excessive and unattenuated angiogenesis occurs in chronic diseases such as inflammation and cancers [5, 6]. Therefore, exploration of prime mechanisms controlling physiological angiogenesis should contribute to maintain the angiogenic balance and alleviate the vascular symptoms in diseases.

The evolutionarily conserved focal adhesion (FA) protein Kindlin-2 is involved in diverse cellular functions such as differentiation, migration, and ECM adhesion. And it is a crucial regulator under both homeostasis and diseased status via regulating a series of signaling pathways. Studies using tissue-specific deletion mouse models have shown that knockout Kindlin-2 in different tissues and organs causes severe phenotypes in bone, intervertebral disk, cartilage, liver, β-cell, smooth muscle and adipose tissue [7–14]. As the FA protein, Kindlin-2 was found to interact with integrin complexes via binding to the cytoplasmic tails of the β subunit. Especially in endothelium, the matrix ligand Vitronectin recognizing endothelial αVβ3 integrin combines with Kindlin-2 which generates outside-in signal to facilitate angiogenesis [15]. Angiogenesis deficiency in Kindlin-2 haploinsufficient mice is mediated by reduced αVβ3 Integrin [16]. After intradermal injection of adeno-associated virus (AAV) to knock down Kindlin-2 expression, mice exhibit delayed skin wound healing and increased vascular permeability [17]. Clinically, high expression of Kindlin-2 in cutaneous melanoma indicates poor prognosis. Activation of mTOR/VEGFA pathway is the underlying mechanism of Kindlin-2 on abnormal angiogenesis in tumor tissues [18]. Altogether, these studies implicate Kindlin-2 as a potential regulator of angiogenesis. However, it remains to demonstrate the role and mechanisms of Kindlin-2 in regulating angiogenesis from endothelium-specific level [19]. Therefore, we aim to decipher the role and mechanisms of endothelial Kindlin-2 in regulating developmental angiogenesis.

Here, we report the important intrinsic role of endothelial Kindlin-2 in regulating cell functions during angiogenesis. Kindlin-2 expression in HUVECs is amplified by pro-angiogenic factor VEGFA stimulation and vice versa. In addition, the indispensability of Kindlin-2 in angiogenesis is further deciphered during embryonic development by using tissue-specific deletion strategy. Mouse embryos exhibit severe hemorrhage and die on E10.5 due to impaired angiogenesis. Notch1, which is activated by VEGFA and in turn restricts VEGFA/VEGFR2 reaction, is identified as an antagonistic target of Kindlin-2 by immunoprecipitation analysis. As a substrate of γ-secretase, Notch1 signaling can be blocked by γ-secretase inhibitor DAPT [20]. The rescue effect of DAPT for angiogenic impairment induced by Kindlin-2 deficiency is demonstrated both in vitro and in vivo.

Our study is of great significance, which indicates that endothelial Kindlin-2 could serve as the angiogenic switch and a potential target for the treatment of angiogenic diseases.

## Materials and methods

### Animal studies

The generation of the *Kindlin-2*$^{fl/fl}$ mice was previously described [10]. The *Tie2-Cre* mice were primarily established as the endothelial-specific receptor tyrosine kinase (Tie2) promoter driving the expression of Cre recombinase [21]. *Tie2-Cre* mice were bred with *Kindlin-2*$^{fl/fl}$ mice to generate *Tie2-Cre; Kindlin-2*$^{fl/fl}$ mice for this study. Pregnant mice were euthanized by compressed $CO_2$ for asphyxiation [22]. Then, embryos were collected at the indicated days after the emergence of vaginal plug date and then photographed by a high-resolution digital camera. The background of all mice used in this project were C57BL/6. Mice were kept at 20–24 °C with a humidity of 40–60% and exposed to

a 12-h light/12-h dark cycle. Protocols for all animal studies were approved by the Institutional Animal Care and Use Committee of Southern University of Science and Technology. The protocols are also in accordance with the National Institutes of Health (NIH) Guidelines for the care and use of laboratory animals. In this study, Primer sequences used in PCR genotyping were listed in Supplementary Table 1.

## Cell culture and cell stimulation

Human umbilical vein endothelial cells (HUVECs) from ATCC (Manassas, VA, USA) were maintained in DMEM/F12 (1:1) growth medium (GIBCO BRL, Grand Island, NY, USA, Cat#: C11330500BT) has no VEGF and contains antibiotics at 37 °C in a 5% $CO_2$ humidified atmosphere [23]. Cells were seeded in complete medium at $3 \times 10^5$ cells per well in 6-well plates for western blotting and qRT-PCR analysis, and at $2 \times 10^4$ cells on glass coverslips in 24-well plates for immunofluorescence staining. For stimulation, human recombinant VEGFA121 (used at 50 ng/ml in all experiments) was obtained from Abcam (Cambridge, MA, USA, Cat#: EPR16637-121). TNFα (used at 50 ng/ml in all experiments) was obtained from Invitrogen (Carlsbad, CA, USA, Cat#: PHC3015). DAPT (used at 10 μM in all experiments) was obtained from (Selleck Chemicals, Houston, TX, USA, Cat#: S2215) [24–26]. IF images were taken using a fluorescence microscope (Nikon confocal A1R with FLIM).

## Cell transfection with siRNA and plasmid

SiRNA sequences targeting human KINDLIN-2 and a negative control (NC) were constructed by GenePharma, Suzhou, China. SiKINDLIN-2 and negative control were transfected into HUVECs with Lipofectamine™ RNAiMAX Transfection Reagent (Invitrogen, Carlsbad, CA, USA, Cat#:13778150) according to standard protocols. For plasmid transfection, NC plasmid or KINDLIN-2 expressing plasmid (OBiO Technology Corp., Ltd, Shanghai, China, Cat#:) were transfected to HUVECs by Lipofectamine™ 3000 Transfection Reagent (Invitrogen, Carlsbad, CA, USA, Cat#: L3000015) according to protocols we previously reported. SiRNA sequences used in this study were listed in Supplementary Table 2.

## Quantitative real-time PCR (qRT-PCR)

Cells were homogenized in Trizol reagent and total RNA was extracted using the RNeasy kit (Vazyme, Nanjing, China, Cat#: RC112-01) following the manufacturer's procedure. Transcripts (1 μg) were reverse-transcribed using high-capacity cDNA Reverse Transcription kit ((Takara, Tokyo, Japan, Cat#: RR047A)). cDNAs were amplified using primers listed in Supplementary Table 3. Finally, qRT-PCR analysis was performed to measure the relative mRNA levels using SYBR Green kit (Bio-Rad Laboratories Inc, Hercules, CA, USA, Cat: 1725124). The expression levels of genes examined were normalized to *GAPDH* expression.

## In situ matrix degradation assay

For the gelatin degradation assay, operations were performed in the dark place. Briefly, glass coverslips were coated with Oregon-green-488 gelatin (Carlsbad, CA, USA, Invitrogen™. Cat. No. G13186) diluted to 0.1% in PBS at RT for 30 min, washed with PBS and fixed with 0.5% glutaraldehyde (Aladdin, Shanghai, China. Cat#: 111-30-8) for 15 min in the dark place. After washing with PBS, coverslips were incubated in 5 mg/ml sodium borohydride (Sigma-Aldrich, St. Louis, MO, USA, Cat#: 452882) for 30 min with agitation (250 rpm) followed by PBS washing for three times and sterilizing by 75% ethanol for subsequent operation. After adhesion, cells were treated with or without VEGFA/DAPT for 24 h, then fixed and processed for immunofluorescence staining. Quantification of degradation areas was performed on 5 randomly picked fields on each coverslip. Then, areas of degradation were quantified by ImageJ software as previously described [27]. Degraded areas were thresholded according to the intensity of the degradation and the loss of matrix-based fluorescence was measured by the Analyze Particles function. Total degradation area ($\mu m^2$) was then normalized to the number of cells (degradation index). Control values were taken as 1.

## Co-immunoprecipitation assay

According to a previously described method [28], IP assays were performed to identify Kindlin2–NICD interactions. Briefly, cultured HEK293T or HUVECs were transiently co-transfected with the plasmids of target genes using transfection reagent (Thermo Fisher Scientific, Waltham, MA, USA, Cat#: 13778-150) according to the manufacturer's instructions. After 48 h, cells were collected and lysed in IP buffer (50 mmol/l Tris–HCl (pH 8.0), 150 mmol/l NaCl, 0.5% sodium deoxycholate, 1% NP-40, and a protease inhibitor cocktail (Roche)) on ice. The cell lysates were primarily precleared with Protein A/G-agarose beads (Thermo, Fisher Scientific, Waltham, MA, USA Cat#: 88802) and then incubated with the corresponding antibodies overnight at 4 °C. The immunocomplex was collected and blotted with indicated 1st and 2nd antibodies. For the ubiquitination assay, HUVECs were co-transfected with HA-ubiquitin constructs and plasmids for 48 h. Then, cells were treated with MG132 (10 μM) for 6 h and harvested in cold IP buffer plus 1% sodium dodecyl sulfate (SDS). Pulled down samples were immunoblotted with corresponding antibodies to detect the polyubiquitinated protein bands under different conditions.

Antibodies used in this study were listed in Supplementary Table 4.

### Tube formation assay

A pre-chilled 96-well plate was filled with 50 µl matrigel (Shanghai Nova Medical Technology Co. Ltd. Ref 082701) without growth factor and incubated at 37 °C for 30 min to let Matrigel coagulates. Thereafter, $2 \times 10^4$ HUVECs in 100 µl complete medium were seeded into each well and incubated at 37 °C for 2–4 h to allow formation of tubular structures and further analyzed by microscopy using a Nikon Eclipse TE2000-E (Nikon Ltd) under 4 × magnification. The angiogenic response was measured by image analysis. The closed polygons and branching points formed were counted manually.

### Wound healing assay

To investigate cell migration, HUVECs were seeded in 24-well plates at the density of $1 \times 10^5$ cell/well, and then cultured in complete medium until confluence. The HUVECs were carefully scratched by a pipette tip (20–200 µl) to create an artificial wound. Cell debris was removed by PBS washing. Then, cells were cultured with serum free medium for 24 h. Phase-contrast figures were acquired to calculate the area of the scratched area.

### IncuCyte ZOOM™ assay

After HUVECs were confluent in 24 well plates, a WoundMaker™ (Essen BioScience) was used to create straight and identical scratches in all wells. Then, the wells were washed twice with pre-warmed PBS to thoroughly remove cell debris and then supplied with serum deprived medium with or without VEGFA. Then, the plate was placed into IncuCyte ZOOM™ live cell imaging system (Essen BioScience, MI USA) and images of the collective cell spreading were captured at 0 h and 24 h. The scratched area was calculated by Image J software.

### Angiogenesis invasion assay (AIA)

AIA was performed as previously reported [6]. After being sterilized, a cut yellow tip was placed in the center of a 3.5 cm confocal dish (JingAn Biological, China) and filled with pure growth factor-reduced Matrigel (66.5 µl) plus 3.5 µl concentration VEGFA to create a BM-like matrix barrier. Matrigel plugs were then allowed to polymerize for 30 min in the incubator at 37 °C, 5% $CO_2$ and the yellow tip was carefully removed. HUVECs ($3 \times 10^5$ cells/dish in 2 ml complete medium) were seeded around the matrigel plot. After overnight incubation, samples were fixed with 2% PFA for 30 min, followed by permeabilization with 0.2% Triton X-100 for 1 h and blockage with 3% BSA for 1 h. Samples were incubated in Alexa fluor-488 labeled phalloidin (Abclonal, Wuhan, China, Cat#: 02836) for 3 h at room temperature. After washing by PBS for 3 × 5 min, the system was then stained with DAPI reagent (Abcam, Cambridge, MA, USA, Cat#: ab104139). To quantify the number of sprouts invading the matrigel plug, mosaic images were obtained by phase-contrast microscope at 4 × magnification. To quantify filopodia number, z-stack series of optical sections (x/y/z = 146.25 × 146.25 × 0.1 µm) were acquired using a laser scanning fluorescence microscope (Zeiss LSM 980 Meta inverted) equipped with a 63X oil immersion objective.

### Immunofluorescence (IF) staining for cells

Sub-confluent cells grown on glass coverslips were fixed for 30 min at room temperature in 4% (w/v) paraformaldehyde, then treated for 15 min at room temperature in permeable solution from Beyotime, 1 h at room temperature in blocking solution from Beyotime, 1 h at room temperature with primary antibodies diluted at 1/100 in blocking buffer. The antibody against Kindlin-2 (MAB2617) is from Millipore (Billerica, MA, USA). HEY1 (A16110) is from Abclonal (Wuhan, China). Cleaved Notch1 (4147S) is from Cell Signaling Technology (Danvers, MA, USA). Then, cells were incubated by fluorescent anti-mouse (Invitrogen, Carlsbad, CA, USA, Cat#: A11008) and anti-rabbit secondary antibodies (Invitrogen, Carlsbad, CA, USA, Cat#: A11036) for 1 h at room temperature. The coverslips were mounted on microscope slides with ProLong Gold Antifade reagent containing DAPI (Abcam, Cambridge, MA, USA, Cat#: ab104139). Images were acquired using a laser scanning fluorescence microscope (Zeiss LSM 980 Meta inverted). Antibodies used in this study were summarized in Supplementary Table 4.

### Histology, immunofluorescence, immunohistochemistry, and confocal analysis

5 µm embryos paraffin sections were used for IHC staining with CD31 (Huabio, Hangzhou, China, Cat#: ER31219) Antibody and the EnVision + System-HRP (DAB) kit (Dako North America Inc, Carpinteria, CA, USA, Cat#:SK-4100). For IF staining, sections were incubated in fluorescent anti-rabbit secondary antibodies (Invitrogen, Carlsbad, CA, USA, Cat#: A11036) and fluorescent anti-rat secondary antibodies (Abclonal, Wuhan, China, Cat#: AS019). Kidneys were isolated from wild type SD rats. Paraffin sections were then used for IF staining with fluorescent anti-rabbit secondary antibodies (Abclonal, Wuhan, China, Cat#: A11036) and fluorescent anti-mouse secondary antibodies (Invitrogen, Carlsbad, CA, USA, Cat#: A11001). Results were acquired

using a laser scanning fluorescence microscope (Zeiss LSM 980 Meta inverted). Methods is as we previously described. Antibodies used in this study were summarized in Supplementary Table 4. All the analyses were done blinded.

## ECs isolation from embryonic mice

Embryos at E10.5 were isolated from maternal mice and sliced into 1–2 mm pieces. Meanwhile, PBS with collagenase (0.5 mg/ml, Type II Collagenase, Worthington, Cat#: CLS-2) was pre-warmed in 37 °C incubator. After being rinsed by PBS, the tissue pieces were incubated for 45 min at 37 °C in 10 ml of pre-warmed PBS with collagenase with shaking until a single cell suspension was obtained. During this incubation, the cells were dissociated at 10-min intervals by pipetting. DMEM (GIBCO by Thermo Fisher Scientific, Waltham, MA, USA, Cat#: 61965059) containing 10% FBS (GIBCO by Thermo Fisher Scientific, Waltham, MA USA, catalog Cat#: 10270106) was added to the cell suspension to neutralize the collagenase activity. Then, cells were gently pelleted, rinsed with PBS and filtered through a 40 mm cell strainer (Corning Life Sciences, Corning, NY USA, Cat#: 352340). Cells were re-suspended in PBS and screened by nano-sized MicroBeads. CD45 MicroBeads (Miltenyi Biotec, Bergisch Gladbach, DE, Cat#: 130-052-301) was primarily used to retain the CD45-negative cell fraction, which was then pelleted and screened by CD31 MicroBeads (Miltenyi Biotec, Bergisch Gladbach, DE, Cat#: 130-097-418). $CD45^{-}/CD31^{+}$ cell fraction is identified as ECs.

## Western blot analyses

Cells were transfected with siRNA as indicated and harvested in Laemmli sample buffer and separated on a 10% SDS-PAGE gel at 80 V for 120 min. Proteins were transferred onto Immobilon polyvinylidene difluoride membranes (Merck Millipore, Billerica, MA, USA, Cat#: ISEQ00010) at 300 mA for 2 h. Membranes were blocked for 1 h in 5% non-fat powdered milk in Tris-buffered saline containing 0.1% Tween 20 at room temperature, followed by an overnight incubation with primary antibodies at 4 °C. Those primary antibodies used for western blotting in this study were summarized in Supplementary Table 4. Then, membranes were incubated with HRP-conjugated anti-mouse (ORIGENE, Rockville, MD, USA, Cat#: ZB2305) or anti-rabbit secondary antibodies ((ORIGENE, Rockville, MD, USA, Cat#: ZB-2301)) for 1 h at room temperature. Finally, blots were developed with an enhanced chemiluminescence (ECL Kit, Millipore Billerica, MA, USA, Cat#: S6010L) and exposed with ChemiDoc XRS chemiluminescence imaging system (Bio-Rad, Hercules, CA, USA). For 9EG7 and 12G10, Western blot analyses were performed using a non-reducing condition [29].

## EdU staining

HUVECs proliferation was measured by a 5-ethynyl-29-deoxyuridine (EdU) incorporation assay. Experiments were conducted according to the manufacturer instructions from the EdU assay kit (RiboBio, Guangzhou, China. Cat#: C10310-1). EdU-labeled cells were manually counted in five randomly selected fields in one 96-well to calculate the positive percentage.

## CCK8 assay

HUVECs in 100 µl medium were treated with DAPT for 24 h and 48 h, 10 µl of CCK-8 solution (AboRo, ShenZhen, Guangdong, China, Cat#: RC0501) was added to each well of the plate. After incubation for 2 h, absorbance at 450 nm was measured using a microplate reader.

## Intravitreal injections and whole retina immunofluorescence

Hypothermia is used to anesthetize C57BL/6J at postnatal day 3 (P3) as previously described [30]. Mice were intravitreally injected with 1 µl of scrambled siRNA, Kindlin2 siRNA, scrambled siRNA + DAPT and Kindlin2 siRNA + DAPT (both siRNAs were from GenePharma, Suzhou, China). All were reconstituted in sterile PBS with 1% DMSO to a final concentration of 1 µg/µl siRNA and 100 µmol/l DAPT.[31, 32] Injections were performed using a 30-gauge needle placed on a 10-µl Nanofl syringe controlled by a UMP3 pump controller. 2 days later (P5), mice were anesthetized as mentioned above for eyeball collection, which were subsequently fixed in 4% paraformaldehyde for 2 h at 4 °C. Retinas were dissected and incubated for 2 h at room temperature in blocking buffer (PBS, 2% BSA, 0.2% Triton X-100). After three washes (each time lasts 20 min) in Pblec buffer (PBS supplemented with 1 mM MgCl2, 1 mM M nCl2, 1 mM CaCl2 and 1% Triton X-100), retinas were incubated overnight at 4 °C with anti-CD31 antibody (Huabio, Hangzhou, China, Cat#: ER31219) diluted in blocking buffer. Then, retinas were washed three times with Pblec buffer and incubated with species-specific fluorescent-labeled secondary antibodies diluted in blocking buffer for 2 h at room temperature. After three washes in PBS, whole retinas were fat-mounted in ProLong Gold Antifade reagent (Life Technologies) containing DAPI and analyzed with a laser scanning fluorescence microscope (Zeiss LSM 980 Meta inverted). Protocols for all animal studies were approved by the Institutional Animal Care and Use Committee of Southern University of Science and Technology. The protocols are also in accordance with the National Institutes

of Health (NIH) Guidelines for the care and use of laboratory animals. SiRNA target sequences used in this study were listed in Supplementary Table 1.

### Statistics

Statistical analysis was performed with GraphPad Prism 8 (GraphPad Software, Inc., San Diego. CA, USA). Data represent at least 5 independent experiments. Graphs are presented as mean values ± SD (bars) and individual values (dots) (scatter plot with bar). Significance was determined by using the Student's *t* test or the two-way ANOVA, followed by Tukey's post-tests. *p* values < 0.05 were considered statistically significant.

## Results

### Kindlin-2 is expressed in endothelial cells

To identify potential roles of Kindlin-2 in angiogenesis, we exposed HUVECs to factors VEGFA and TNFα, which are important for angiogenesis [33, 34], and measured the expression level of KINDLIN-2 in HUVECs. After exposed to VEGFA, KINDLIN-2 expression in HUVECs was significantly elevated at both mRNA level and protein level (Fig. 1A–C). On the contrary, its expression was significantly suppressed after TNFα treatment (Fig. 1D–F). Thus, these results suggested that Kindlin-2 might be involved in in vitro angiogenesis. Using immunofluorescence staining, we then explored the in vivo expression of Kindlin-2 in ECs of rat kidneys. Kindlin-2 is extensively distributed in various solid tissues [11, 35] and the result showed that CD31 positive ECs were also positive for Kindlin-2 expression (Fig. 1G). Based on the above findings, we aim to demonstrate the roles of endothelial Kindlin-2 in angiogenesis.

### Kindlin-2 is indispensable for physiological angiogenesis

To investigate the in vivo role of Kindlin-2 in angiogenesis, we crossed *Kindlin-2*$^{fl/fl}$ mice to *Tie2-Cre* mice to specifically delete Kindlin-2 in ECs (*Tie2-Cre; Kindlin-2*$^{fl/fl}$ mice, referred to as cKO hereafter). From a total of 187 mice (from 33 l), no live cKO mice (1/4 probability, based on Mendel's laws of inheritance) were born, indicating that these mice die during embryogenesis. Embryos were then collected at different time points after mating. At E9.5, the cKO embryos

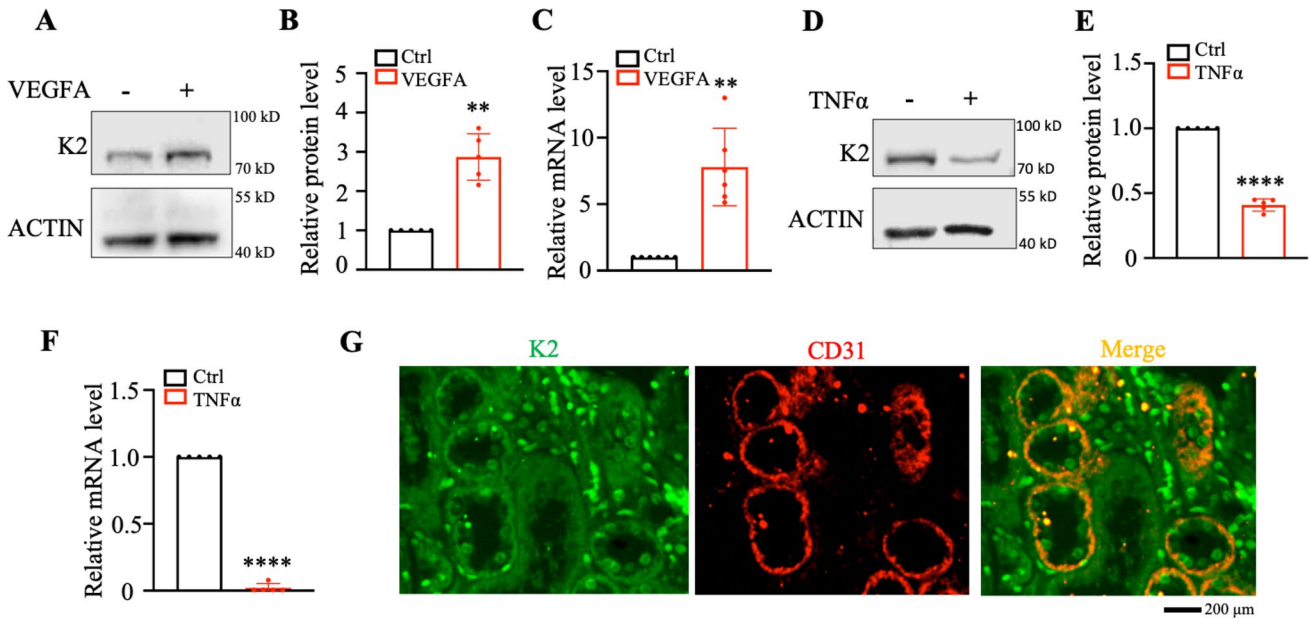


**Fig. 1** Kindlin-2 is strongly expressed in endothelial cells. **A, B** HUVECs were treated by VEGFA (50 ng/ml) or not for 24 h and cell extracts were prepared. Representative Western blotting results show increased protein level of KINDLIN-2 in VEGFA-stimulated HUVECs ($N=5$ independent experiments, mean ± SD is shown. Student' *t* test, $^{**}p<0.01$ vs control). **C** QRT-PCR results show increased mRNA level of KINDLIN-2 in VEGFA-stimulated HUVECs ($N=6$ independent experiments, mean ± SD is shown. Student' *t* test, $^{**}p<0.01$ vs control). **D, E** HUVECs were treated by TNFα (50 ng/ml) or not for 48 h and cell extracts were prepared. Representative Western blotting results show reduced protein level of KINDLIN-2 in TNFα-stimulated HUVECs ($N=5$ independent experiments, mean ± SD is shown. Student' *t* test, $^{****}p<0.0001$ vs control). **F** qRT-PCR results show reduced mRNA level of KINDLIN-2 in TNFα-stimulated HUVECs ($N=5$ independent experiments, mean ± SD is shown. Student' *t* test, $^{****}p<0.0001$ vs control). **G** Co-localization of CD31 and KINDLIN-2 was detected in the kidney vasculature of rats. Scale bars: 200 μm

appeared no observable differences; however, at E10.5, the cKO embryos exhibited impaired angiogenesis compared with the control ones (Fig. 2A). And at E10, the cKO mice still had heartbeat (Supplementary video), suggesting that the cKO embryos died from impaired angiogenesis rather than from heart failure. Deletion of endothelial Kindlin-2 induced hemorrhage at E10.5 because of the insufficient vasculature (Fig. 2B), and there was no heartbeat detected at this time point. At E11.5, mutant embryos exhibited embryonic shrinkage (Fig. 2A). To further examine the cause of hemorrhage of cKO embryos at E10.5, we sectioned the embryos and stained with anti-CD31 antibody to identify vessels. Compared with negative controls, IHC staining revealed that vascular structure was irregular and disordered in the embryonic tissues of cKO mice (Fig. 2C). Therefore, ECs lacking Kindlin-2 in vivo had no capacity of morphogenesis and led to aberrant embryonic development. The co-localization of CD31 and Kindlin-2 illustrated the successful deletion of endothelial Kindlin-2 in sections of cKO embryos which caused insufficient vasculature (Fig. 2D). It is reported that Tie2 is also expressed in pericytes; however, the level is much lower than in ECs [36]. Since pericytes also contribute to angiogenesis and NG2 is the marker of pericytes [37], we detected the expression of Kindlin-2 in $NG2^+$ cells in embryos of control group and cKO group to determine if Kindlin-2 expression in pericytes was affected in cKO mice. Results showed that the co-localization between Kindlin-2 and NG2 was not evidently changed (Fig. S1). Thus, the above results establish the indispensable intrinsic role of endothelial Kindlin-2 in regulating developmental angiogenesis.

## Kindlin-2 regulates endothelial basement membrane degradation and cell sprouting

To further explore the fundamental roles of Kindlin-2 in angiogenesis, we altered KINDLIN-2 levels in HUVECs and evaluated the variation of their features in vitro. Characterized by the basement membranes (BMs) proteolysis caused by invasive tip cells [38], the primary stage of angiogenesis is matrix proteolytic response. Using green fluorescence labeled gelatin, we examined the matrix degradation capacity of cells with altered KINDLIN-2 by the measurement of black areas from the green fluorescence [6]. After being transfected by KINDLIN-2 overexpressing plasmid or siRNA, which was verified by Western blotting (Figs. S2L, 3J). HUVECs were seeded on green gelatin and stimulated with VEGFA or not, respectively. Compared with the control group, cells with KINDLIN-2 overexpression degraded more gelatin, and it was not further strengthened by VEGFA treatment (Fig. S2A, B). KINDLIN-2 Knockdown showed an opposite result (Fig. 3A, B). Furthermore, using 3D angiogenesis invasion assay (AIA), we examined whether Kindlin-2 participate in the specification between tip cells and stalk cells. Matrigel plug deprived of growth factors was supplemented with VEGFA and was set in the central tank of the culture dish. Confluent HUVECs were seeded around matrigel in a monolayer manner and generated endothelial sprouts along the matrigel-HUVECs interface [6]. In response to VEGFA stimulation, these tip-cell like structures can stretch out filopodias and invade into Matrigel [6]. Apparently, ECs formed sprouts at a higher frequency with KINDLIN-2 overexpression (Fig. S2C–F). By taking the advantage of assembling more filopodias, endothelial sprouts of ECs richer in KINDLIN-2 were more prone to migrate toward VEGFA origin and embodied as longer sprouts. Conversely, KINDLIN-2 knockdown reduced the length and quantity of invasive sprouts (Fig. 3C–F), indicating an overall shortage of sprouting angiogenesis. Based on these results, we hypothesized that the diverse invasion extent of KINDLIN-2 overexpressing cells in matrigel may be caused by the alteration of VEGFA-induced chemotaxis.

## Kindlin-2 regulates endothelial cell migration and tube formation in vitro

Given that the number and length of endothelial sprouts in matrigel are positive to KINDLIN-2 expression, next we performed wound healing assay to assess migration ability of HUVECs through the operation of incucyte. Compared with control group, cells overexpressing KINDLIN-2 exhibited faster healing of artificial gaps between two confluent cell crowds. Compared with positive control, VEGFA failed to further accelerate the wound healing of cells rich in KINDLIN-2 (Fig. S2G, H). After breaking through the obstacles of BMs and interstitial components, activated ECs form tube-like structures in the late stage of angiogenesis after producing and adhering to the BMs constituents. The morphogenesis is crucial to form the trunk of neo-vessels and is simulated in vitro by seeding ECs on matrigel, which is the BMs-mimic structure. Being immersed in matrigel, ECs are aligned end-to-end and elongate to form network by anastomosing function [6]. Results in Fig. S2I–K showed that the above process was promoted by the overexpression of endothelial KINDLIN-2, which was verified by Western blotting (Fig. S2L). In contrast, compared with the control group, confluent HUVECs with KINDLIN-2 knock down failed to merge the gap timely in wound healing assay (Fig. 3G, H). Furthermore, sub-confluent HUVECs with KINDLIN-2 knockdown had impaired migration even though under the stimulation of VEGFA. And HUVECs with KINDLIN-2 knockdown lost the tube formation competence (Fig. 3I). The transfection effect of siRNA KINDLIN-2 was shown in Fig. 3J. Altogether, endothelial impairment induced by the absence of KINDLIN-2 was not efficiently recovered with the involvement of VEGFA. In conclusion,

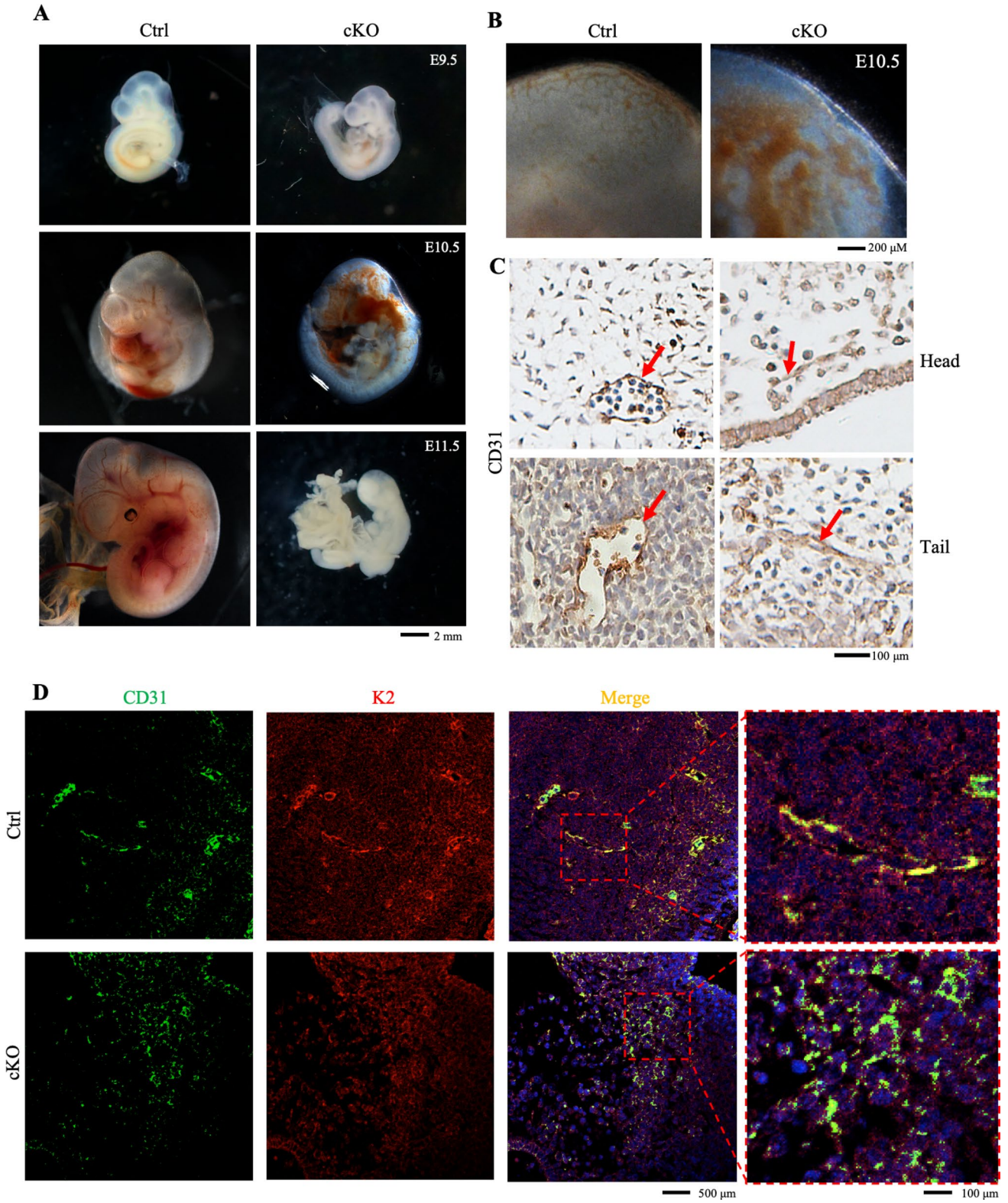


**Fig. 2** Kindlin-2 specific deletion in endothelial cells causes embryonic lethality of mice. **A** *Tie2-cre; Kindlin-2*$^{fl/fl}$ (cKO) and *Kindlin-2*$^{fl/fl}$ (Ctrl) embryos collected at E9.5, E10.5 and E11.5. $N=8$ embryos in each group. Scale bars: 2 mm. **B** Vasculature in *Tie2-cre; Kindlin-2*$^{fl/fl}$ (cKO) *and Kindlin-2*$^{fl/fl}$ (Ctrl) embryos at E10.5. $N=8$ embryos in each group. Scale bars: 200 μm. **C** IHC staining of E10.5 embryos with CD31, sections shown are the head and tail parts of embryos. $N=4$ embryos in each group. Scale bars: 100 μm. **D** Immunofluorescent staining of E10.5 embryos with CD31 (green) and Kindlin-2 (red). Sections shown are the back part of embryos. $N=4$ embryos in each group. Scale bars: 500 μm and 100 μm

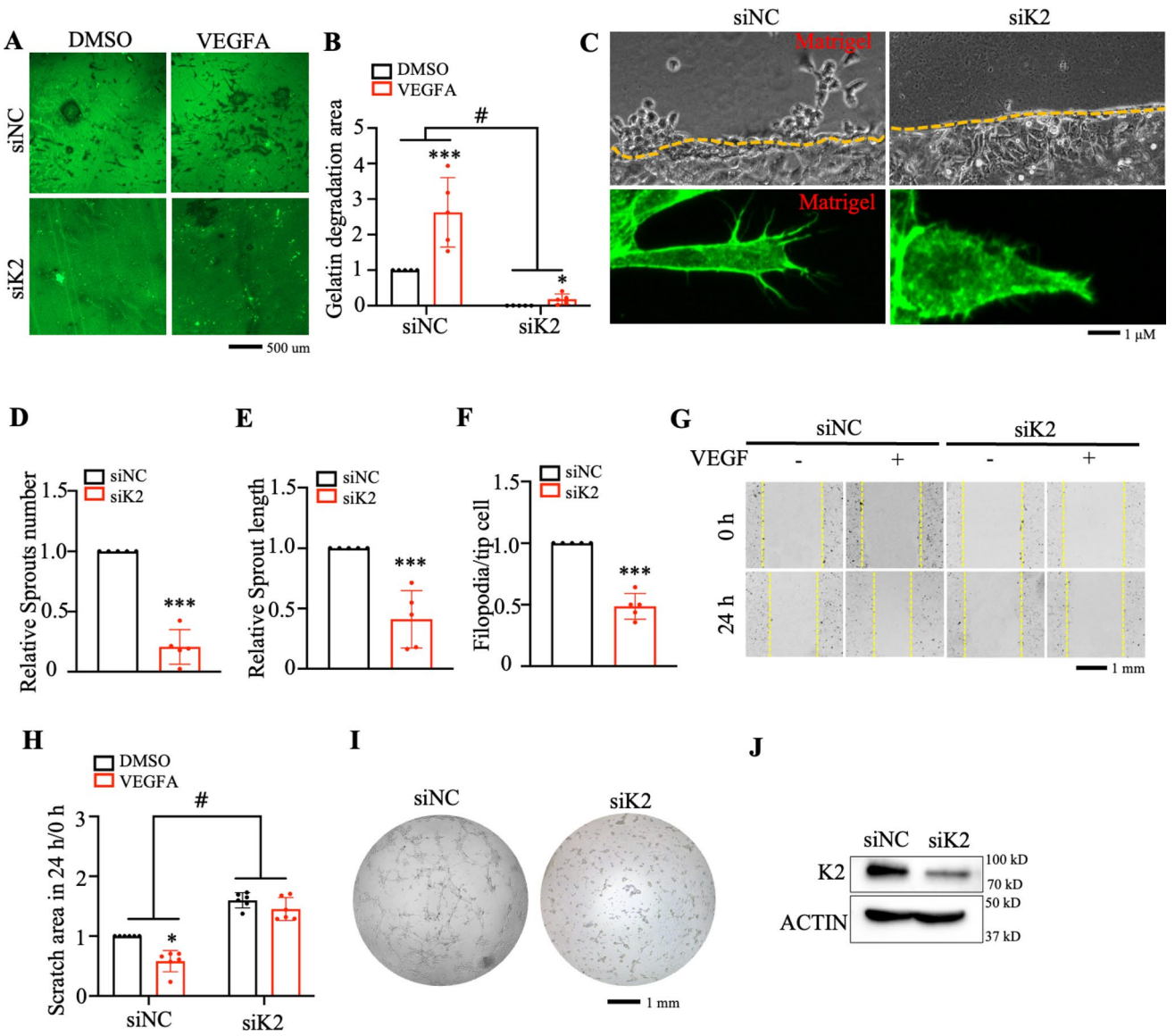


**Fig. 3** Kindlin-2 deficiency impairs endothelial basement membrane degradation, cells sprouting, migration, and tube formation. **A, B** Representative images of gelatin degradation of HUVECs transfected with siNC and siK2 ($N=6$ independent experiments, mean ± SD is shown. $^{***}p<0.001$, vs siNC. Two-way ANOVA Bonferroni multiple comparison test, $^{\#}p<0.05$). Scale bars: 500 μm. **C** Higher magnification images show ECs sprouting into matrigel and filopodias on activated sprouts. Scale bars: 1 μm. Statistics of number (**D**) and length (**E**) of ECs sprouts ($N=6$ independent experiments, mean ± SD is shown. Student' $t$ test, $^{***}p<0.001$ vs siNC). Statistics of filopodias assembled on sprouts (**F**) ($N=6$ independent experiments, mean ± SD is shown. Student' $t$ test, $^{***}p<0.001$ vs siNC). **G** Representative phase-contrast images taken at 0 h and 24 h after scraping the confluent monolayer cells showed the wound width and their statistics (**H**) ($N=8$ independent experiments, mean ± SD is shown. $^{*}p<0.05$, vs siNC. Two-way ANOVA Bonferroni multiple comparison test, $^{\#}p<0.05$). Scale bars: 1 mm. **I** Representative images of tube formation. $N=5$ independent experiments. Scale bars: 1 mm. **J** Western blotting results of KINDLIN-2 in HUVECs transfected by siK2 or siNC. $N=5$ independent experiments

the KINDLIN-2-dependent endothelial properties that we analyzed from 2D cultured HUVECs were in accordance with sprouting behaviors in 3D assays in vitro. Thus, the decisive effect of Kindlin-2 on each stage of sprouting angiogenesis was clearly demonstrated in this study.

Kindlin-2 is one of the crucial proteins of focal adhesions, which is critical in regulating integrin activation. Therefore, we examined if the expression or activation of β1 integrin was regulated by Kindlin-2 alteration. We isolated ECs from embryos at E10.5 and tested the deleting efficiency of Kindlin-2. WB analyses showed that protein level of Kindlin-2 was evidently decreased in ECs of cKO mice compared with that of control mice. However, the activation of mouse β1 integrin (9EG7) [29, 39, 40] was not changed (Fig.

S3A and D). WB analyses revealed that the activation of hominine β1 INTEGRIN (12G10) [41] was not affected by KINDLIN-2 knockdown or overexpression (Fig. S3B and C). Furthermore, we examined if the level of the other two KINDLIN family members, KINDLIN-1 or KINDLIN-3 was regulated by KINDLIN-2 alteration in HUVECs. We found that KINDLIN-3 was positively regulated by KINDLIN-2, indicating no compensatory expression of KINDLIN-3 in response to KINDLIN-2 knockdown. KINDLIN-1 was increased when KINDLIN-2 was knocked down and KINDLIN-1 was decreased when KINDLIN-2 was overexpressed in HUVECs (Fig. S3E and F), indicating that there were compensatory alterations in Kindlin-1 expression associated with alterations of Kindlin-2 levels. Moreover, as an important angiogenic factor and downstream protein of Notch signaling [42–44], TWIST was negatively regulated by KINDLIN-2 in HUVECs (Fig. S3G). Meanwhile, compared with control embryos, the protein level of Twist in ECs of cKO embryos was also increased (Fig. S3H).

## Endothelial Kindlin-2 controls angiogenic competence via Notch1 signaling

Preceding results displayed that the angiogenic functions of HUVECs strongly lie on KINDLIN-2. Angiogenic occurrence relies on the correct specification between tip cells and stalk cells. During angiogenesis, specification between tip cells and stalk cells is orchestrated by VEGF/Notch1 pathway. Initiation of Notch1 signal is derived from the cleavage and production of Notch1 intracellular domain (NICD), and subsequent transcriptional activation of *Hey1* and *Hes1*, etc. [45–47]. The unbalance of this negative feedback loop causes pathological angiogenesis and aberrant vasculature [48–50]. Therefore, we estimated the possible relationship between VEGF/Notch1 pathway and Kindlin-2 during vascular growth. HUVECs with KINDLIN-2 overexpression exhibited lower levels of NICD, HEY1 and HES1, while NOTCH1 was increased (Fig. S4A, B). qRT-PCR analyses revealed that *HES1* and *HEY1* but not *NOTCH1* were reduced at mRNA level by KINDLIN-2 overexpression (Fig. S4C). In addition, the suppression effect of KINDLIN-2 on crucial proteins of NOTCH1 pathway was also demonstrated through immunofluorescence (IF) staining (Fig. S4D–F). EdU staining showed that proliferation of HUVECs with KINDLIN-2 overexpression was decreased, which was possibly mediated by the impaired NOTCH1 pathway [51, 52] (Fig. S4G, H). On the contrary, inhibition of KINDLIN-2 promoted NOTCH1 pathway, and cellular proliferation (Fig. 4A–H). Mice suffered from endothelial Kindlin-2 deletion only survived to E10.5. We stained the sections of E10.5 embryos with antibodies against CD31 and Notch1 signaling proteins. Compared with the control group, more NICD, Hey1 or Hes1 were detected in CD31 positive cells, which was accompanied by impaired vasculature in mutant embryos (Fig. 4I–K). Therefore, strengthened Notch1 signal is responsible for the vascular deficiency in the absence of endothelial Kindlin-2. Altogether, by inhibiting Notch1 pathway, Kindlin-2 plays an essential role in angiogenesis both in vivo and in vitro.

## Kindlin-2 limits Notch1 signaling by interacting with NICD and preventing the cleavage of Notch1

We further determined how Kindlin-2 modulates Notch1 signaling. IF staining revealed the co-localization of KINDLIN-2 and NOTCH1 or NICD in HUVECs (Fig. 5A). Next, immunoprecipitation (IP) assays demonstrated that KINDLIN-2 interacted with NICD in HEK293T cells by protein overexpression (Fig. 5B, C). Moreover, interaction of endogenous KINDLIN-2 and NICD was also confirmed in HUVECs (Fig. 5D, E). Proteasome-mediated protein degradation is one of the main pathways for protein degradation within cells. We then examined if the interaction between KINDLIN-2 and NICD would affect NICD stability. HUVECs were treated with MG132, which blocked the proteasome degradation pathway and led to accumulation of KINDLIN-2 and NICD proteins. Results showed that KINDLIN-2 knockdown increased NICD protein level both in presence or absence of MG132 (Fig. 5F, G), indicating that NICD was degraded by proteasome-mediated pathway, and MG132 treatment didn't affect NICD increase in ratio caused by KINDLIN-2 deficiency. Cycloheximide (CHX) experiment showed that KINDLIN-2 knockdown had no obvious effect on NICD protein stability but the initial production in HUVECs (Fig. 5H, I). Treatment of DAPT, a known γ-secretase inhibitor [53], totally blocked the NICD enhancing effect of Kindlin-2 deficiency (Fig. 5J, K). To identify which region of Kindlin-2 molecule is essential for the interaction with NICD, a serials of Kindlin-2 deletion plasmids were constructed and transfected into HEK293T cells, followed by IP assays. Results showed that KINDLIN-2 fragment of aa 1–569 region sustained the interaction between NICD and KINDLIN-2. Fragment of aa 570–680 or 1–239 abolished the interaction above, indicating that KINDLIN-2 fragment aa 240–560 is necessary for NICD interaction (Fig. 5L). Collectively, these data demonstrate that KINDLIN-2 decreases NICD production through binding to and preventing the cleavage of NOTCH1 to release NICD without affecting NICD protein stability.

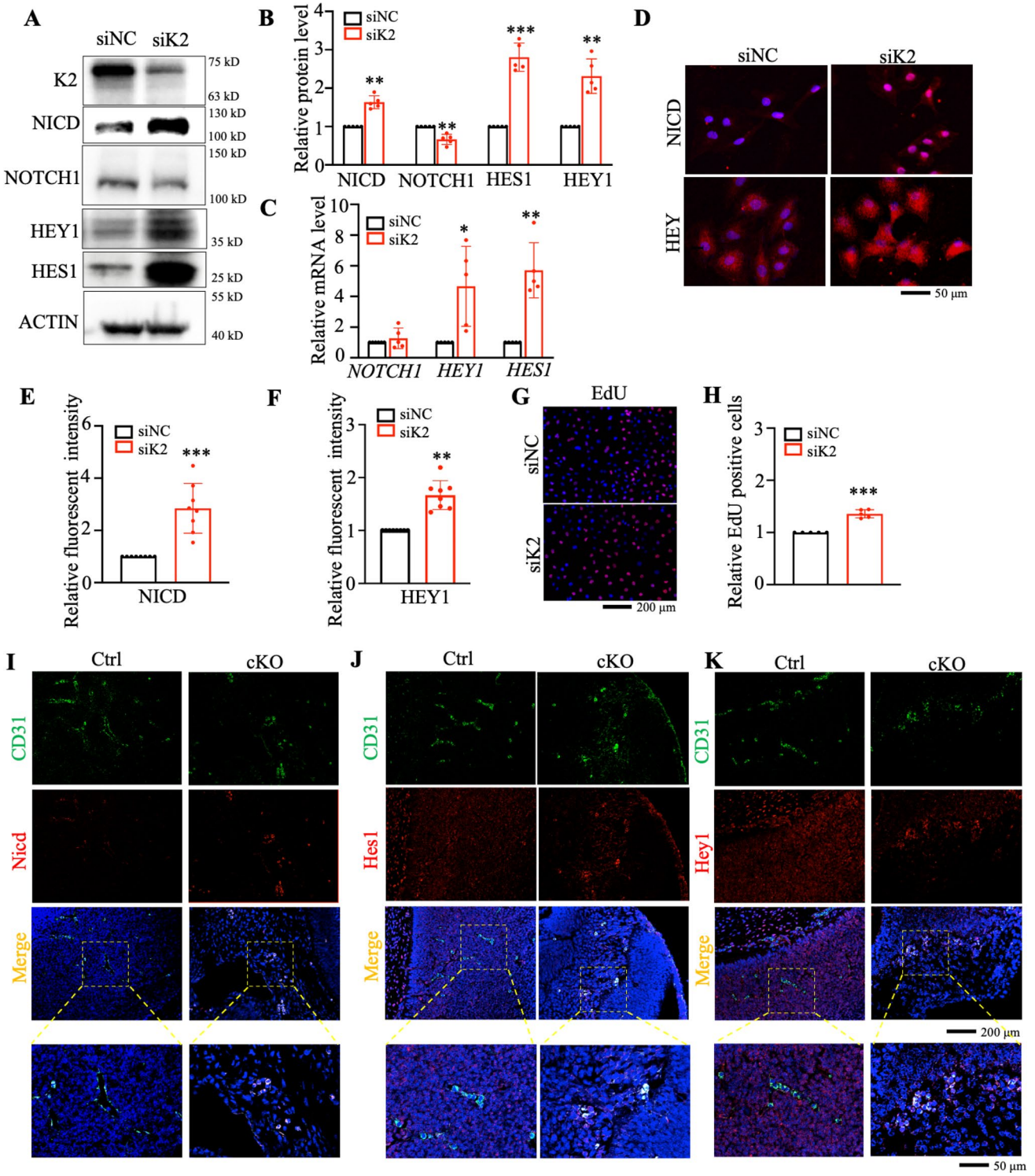


**Fig. 4** Endothelial KINDLIN-2 controls angiogenic competence via NOTCH1 signaling. **A, B** Western blotting results of NICD, HEY1, HES1 and NOTCH1 in KINDLIN-2 siRNA transfection group (siK2) or control group (siNC) ($N=5$ independent experiments, mean ± SD is shown. Student' $t$ test, $^{**}p<0.01$, $^{***}p<0.001$ vs siNC). **C** qRT-PCR of *NICD*, *HEY1* and *HES1* ($N=5$ independent experiments, mean ± SD is shown. Student' $t$ test, $^{*}p<0.05$, $^{**}p<0.01$, $^{***}p<0.001$ vs siNC). **D–F** Immunofluorescence staining and fluorescence intensity of NICD and HEY1 ($N=8$ independent experiments, mean ± SD is shown. Student' $t$ test, $^{**}p<0.01$, $^{***}p<0.001$ vs siNC). Scale bars: 50 μm. **G, H** Proliferation reflected by EdU positive cells ($N=5$ independent experiments, mean ± SD is shown. Student' $t$ test, $^{***}p<0.001$, vs siNC). Scale bars: 200 μm. **I–K** Immunofluorescence of NICD, Hey1 or Hes1 (red) co-staining with CD31 (green) in mouse embryos of *Tie2-cre; Kindlin-2*$^{fl/fl}$ (cKO) and *Kindlin-2*$^{fl/fl}$ (Ctrl). $N=5$ independent experiments. Scale bars: 200 μm

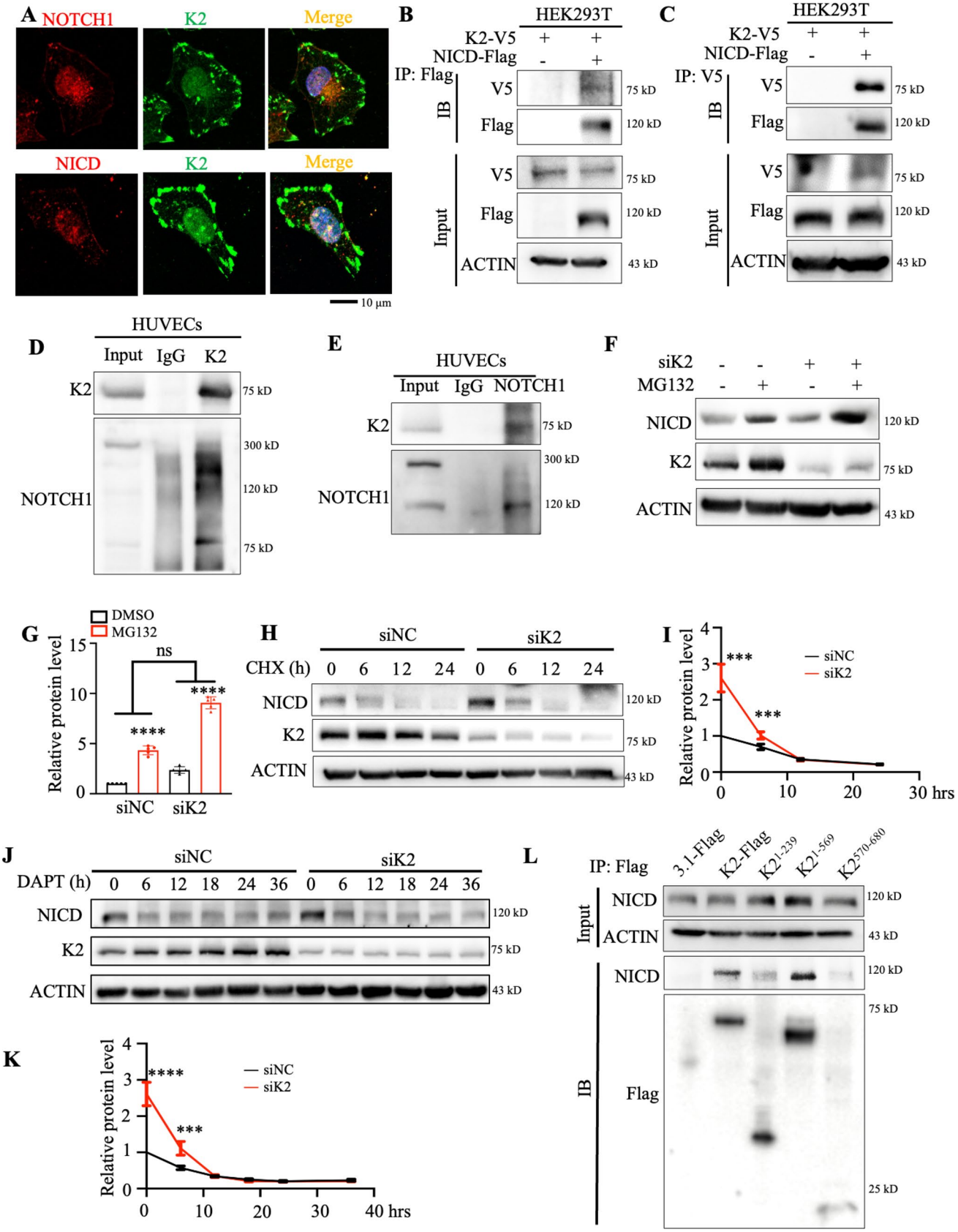
A
NOTCH1
K2
Merge
NICD
K2
Merge
10 μm
B
HEK293T
K2-V5 + +
NICD-Flag - +
IP: Flag
IB
V5
Flag
Input
V5
Flag
ACTIN
75 kD
120 kD
43 kD
C
HEK293T
K2-V5 + +
NICD-Flag - +
IP: V5
IB
V5
Flag
Input
V5
Flag
ACTIN
75 kD
120 kD
43 kD
D
HUVECs
Input IgG K2
K2
NOTCH1
75 kD
300 kD
120 kD
75 kD
E
HUVECs
Input IgG NOTCH1
K2
NOTCH1
75 kD
300 kD
120 kD
F
siK2 - - + +
MG132 - + - +
NICD
K2
ACTIN
120 kD
75 kD
43 kD
G
DMSO
MG132
Relative protein level
15
10
5
0
ns
****
****
siNC
siK2
H
siNC
siK2
CHX (h) 0 6 12 24 0 6 12 24
NICD
K2
ACTIN
120 kD
75 kD
43 kD
I
Relative protein level
4
3
2
1
0
***
***
siNC
siK2
0
10
20
30 hrs
J
siNC
siK2
DAPT (h) 0 6 12 18 24 36 0 6 12 18 24 36
NICD
K2
ACTIN
120 kD
75 kD
43 kD
K
Relative protein level
4
3
2
1
0
****
***
siNC
siK2
0
10
20
30
40 hrs
L
IP: Flag
3.1-Flag
K2-Flag
K2 1-239
K2 1-569
K2 570-680
Input
NICD
ACTIN
IB
NICD
Flag
120 kD
43 kD
120 kD
75 kD
25 kD

◂**Fig. 5** KINDLIN-2 sustains the NOTCH1 stability by interacting with NICD and preventing the cleavage of NOTCH1. **A** Immunofluorescence staining of NOTCH1 or NICD (red) and KINDLIN-2 (green) of HUVECs. $N=6$ independent experiments. Scale bars: 10 μm. **B, C** Co-IP assays of V5-NICD and Flag-KINDLIN-2 in HEK293T cells. $N=5$ independent experiments. **D, E** co-IP assays of NICD and KINDLIN-2 in HUVECs. $N=5$ independent experiments. **F, G** MG132 assays of HUVECs transfected by siNC and siK2. The cells were pre-treated by MG132 (10 μg) for 6 h before harvested. $N=5$ independent experiments. **H, I** CHX (100 μg/ml) experiments of HUVECs transfected with siK2 or siNC, samples were harvested at various time points. Protein level of NICD was examined by Western Blotting. $N=5$ independent experiments. **J, K** DAPT treatment of HUVECs transfected with siK2 or siNC, samples were harvested at different time points. Protein level of NICD was detected by Western Blotting. $N=5$ independent experiments. **L** CO-IP assays of NICD and full-length or truncated KINDLIN-2, HUVECS were transfected with full-length or truncated KINDLIN-2 for 48 h, and cell extracts were harvested for CO-IP assays. $N=5$ independent experiments

## DAPT treatment reverses the impaired angiogenic functions of HUVECs caused by endothelial KINDLIN-2 inhibition

Through intensifying the NOTCH1 pathway, KINDLIN-2 deficient HUVECs hardly degrade the surrounding matrix components, migrate, and generate tubular structures. Next, we examined if NOTCH1 inhibitor DAPT could reverse the impaired angiogenesis capacity of HUVECs caused by KINDLIN-2 deficiency. Firstly, we stimulated HUVECs with DAPT for 24 h and 48 h. The morphology of HUVECs was not changed, and CCK8 assay demonstrated that DAPT had no obvious cytotoxicity (Fig. S5H, I). Results showed that the increase of NICD, HEY1, HES1 caused by KINDLIN-2 knock down was reversed by the treatment of DAPT (Fig. 6A–E). Subsequently, we also demonstrated that the decreased degradation of matrix, migration, formation of tube-like structures and sprouting by HUVECs deficient of KINDLIN-2 were reversed by DAPT treatment (Figs. 6I, S5A–G). In the absence of KINDLIN-2, the increased protein level of NICD in nucleus and HEY1 in cytoplasm were reversed by the DAPT treatment (Fig. 6F–H). Collectively, these results indicate that acute blockage of NOTCH1 signal in ECs at least partially rescues the angiogenic dysfunction caused by KINDLIN-2 deficiency.

Since the impaired angiogenic functions of HUVECs caused by KINDLIN-2 deficiency could be reversed by DAPT treatment, we further explored the inhibitory effect of DAPT in retinas vascular network. Vascular plexus of neonatal mice originates from optic nerves and extends to the periphery of retinas. Vascular network can cover all the surface layer of retinas at P7 [54, 55]. Intravitreal injection of siKindlin-2 and DAPT were performed at P4. Results showed that after 48 h, retinal angiogenesis of P6 mice was dramatically inhibited by Kindlin-2 inhibition revealed by IF staining of CD31, which could be largely rescued by DAPT treatment (Fig. 6J).

Altogether, these data demonstrate that pathological angiogenesis manifested as excessive sprouting could be prevented by endothelial Kindlin-2 inhibition. Finally, Kindlin-2 regulation of angiogenesis and the underlying mechanism was depicted in the diagram (Fig. 6K).

## KINDLIN-2 deficiency attenuates excessive angiogenesis caused by high glucose (HG) treatment

To evaluate whether targeting endothelial Kindlin-2 can prevent excessive angiogenesis induced by HG, we performed the in vitro HG model. Results showed that KINDLIN-2 in HUVECs was increased by HG (Fig. 7A–D). Due to the positive relationship between the level of Kindlin-2 and angiogenesis demonstrated in this study, vascular overgrowth occurs during HG treatment is possibly caused by increased expression of endothelial KINDLIN-2. To confirm the hypothesis, we performed HG treatment on HUVECs with or without KINDLIN-2 knockdown. The strengthened functions of HUVECs by HG treatment, such as gelatin degradation, migration and morphogenesis, were disrupted by the inhibition of endothelial KINDLIN-2 (Fig. 7E–I). In 3D cultured system, KINDLIN-2 deficiency reversed the increase of number, length and filopodia assembly of endothelial sprouts in HG-treated HUVECs (Fig. 7J–N).

# Discussion

Although previous studies have suggested the potential role of Kindlin-2 in angiogenesis, the role of Kindlin-2 in developmental angiogenesis has not been reported from the endothelial level. Our work represents the first systematic study of the functions of Kindlin-2 in developmental angiogenesis. In this study, we decipher that endothelial Kindlin-2 determines the dynamic switch between tip cells and stalk cells by interacting with Notch directly to modulate developmental angiogenesis. The critical roles of endothelial Kindlin-2 in angiogenesis defined in our study highlight the possibility of Kindlin-2 as a potential target for the treatment of angiogenic diseases.

Our first purpose is to verify the indispensable roles of endothelial Kindlin-2 during developmental angiogenesis in vivo. We failed to obtain any live cKO mice since they died at E10.5. This phenomenon overwhelmingly supports

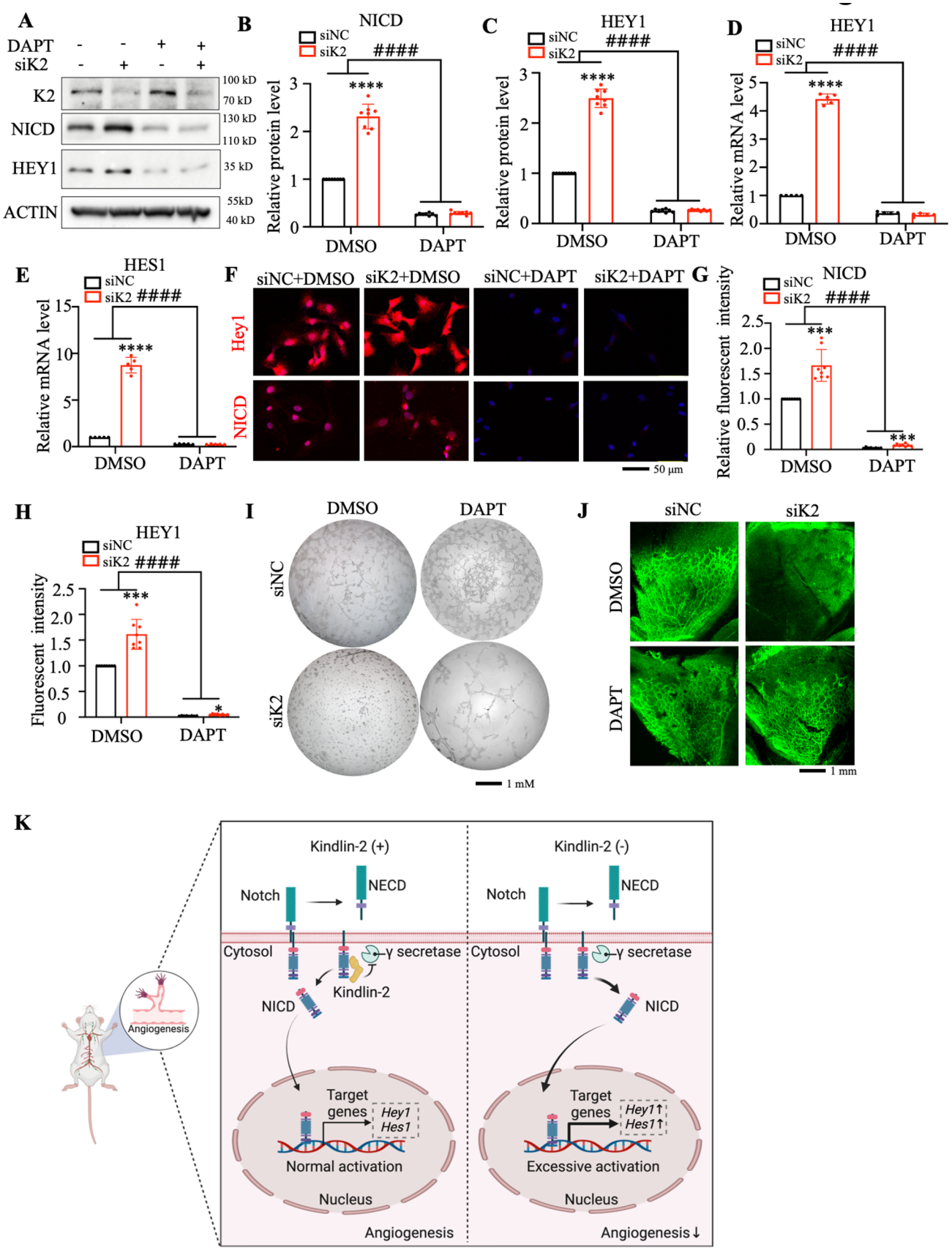
A
DAPT - - + +
siK2 - + - +
K2
NICD
HEY1
ACTIN
100 kD
70 kD
130 kD
110 kD
35 kD
55kD
40 kD
B
NICD
siNC
siK2
####
****
Relative protein level
DMSO
DAPT
C
HEY1
siNC
siK2
####
****
Relative protein level
DMSO
DAPT
D
HEY1
siNC
siK2
####
****
Relative mRNA level
DMSO
DAPT
E
HES1
siNC
siK2 ####
****
Relative mRNA level
DMSO
DAPT
F
siNC+DMSO
siK2+DMSO
siNC+DAPT
siK2+DAPT
Hey1
NICD
50 μm
G
NICD
siNC
siK2
####
***
***
Relative fluorescent intensity
DMSO
DAPT
H
HEY1
siNC
siK2 ####
***
*
Fluorescent intensity
DMSO
DAPT
I
DMSO
DAPT
siNC
siK2
1 mM
J
siNC
siK2
DMSO
DAPT
1 mm
K
Kindlin-2 (+)
Kindlin-2 (-)
Notch
NECD
Cytosol
γ secretase
Kindlin-2
NICD
Target genes
Hey1
Hes1
Hey1↑
Hes1↑
Normal activation
Excessive activation
Nucleus
Angiogenesis
Angiogenesis↓

◂**Fig. 6** Impaired angiogenic functions caused by endothelial KINDLIN-2 inhibition is reversed by treatment of NOTCH inhibitor DAPT. **A–C** Western blotting of NICD, HEY1. HUVECs were transfected with siK2 or siNC for 48 h and treated with or without DAPT ($N=5$ independent experiments, mean ± SD is shown. $^{**}p<0.01$, $^{***}p<0.001$, $^{****}p<0.0001$ vs siNC. Two-way ANOVA Bonferroni multiple comparison test, $^{\#\#\#\#}p<0.0001$). **D, E** qRT-PCR of *HEY1* and *HES1*. HUVECs were transfected with siK2 or siNC for 48 h and treated with or without DAPT ($N=5$ independent experiments, mean ± SD is shown. $^{****}p<0.001$ vs siNC. Two-way ANOVA Bonferroni multiple comparison test, $^{\#\#\#\#}p<0.0001$). **F–H** Immunofluorescent staining of NICD and HEY1. Cells transfected with siK2 or siNC for 48 h and treated with or without DAPT ($N=8$ independent experiments. mean ± SD is shown. $^{*}p<0.05$, $^{***}p<0.001$, vs siNC. Two-way ANOVA Bonferroni multiple comparison test, $^{\#}p<0.05$, $^{\#\#\#\#}p<0.0001$). Scale bars: 50 μm. **I** Tube formation of HUVECs, cells were transfected with siK2 or siNC for 48 h and treated with or without DAPT. $N=4$ independent experiments. Scale bars:1 μM. **J** CD31 stained retinal wholemounts from P6 mice. Intravitreally injected with the siNC, siK2 or DAPT at P4. $N=4$ mice in each group. Scale bars: 1 mm. **K** Working model of Kindlin-2 limiting Notch1 signaling. During angiogenesis, endothelial Notch1 is cleaved by γ-secretase. Free Notch1 Intracellular Domains (NICD) are transferred to nucleus to direct the transcription of *Hey1* and *Hes1*. Kindlin-2 interacts with NICD and prevents the cleavage of Notch1. In contrast, Kindlin-2 deficiency facilitates Notch1 signal

our results of in vitro experiments, which clearly reveal the impaired angiogenic capacity of HUVECs caused by KINDLIN-2 deficiency. Hierarchical plexus generated during embryonic development is achieved by two dynamic and distinct processes: vasculogenesis and angiogenesis [56]. Unlike angiogenesis occurring in the pre-existing vessels, vasculogenesis refers to de novo assembly of vessels. Angioblasts, originated from lateral plate mesoderm, can be organized into cord-like primitive vessels, which are expanded to fulfill the mature network. The growth of embryonic mice from E6.5 to E9.5 is nourished by vasculogenesis and then by angiogenesis [57]. In consideration of the similar embryonic morphology between cKO and control embryos at E9.5, it is possible that angioblasts are not affected by Kindlin-2 deletion in endothelial cells and the cKO embryos have normal vasculogenesis before E9.5. However, for the following angiogenesis, the cKO embryos cannot form neo-vessels effectively to ensure survival and die at E10.5.

The role of Kindlin-2 in regulating angiogenesis arouses our interest because of the varying KINDLIN-2 expression in HUVECs after treated with angiogenic factors. Results strongly demonstrate that adequate endogenous KINDLIN-2 in HUVECs guarantees matrix degradation, migration and tube formation capacities required for sprouting angiogenesis [58]. We for the first time establish the direct inhibition of Kindlin-2 on Notch1 pathway, which serves as the underlying mechanism above. Conversely, rescuing effect of Notch1 inhibition on angiogenic impairment caused by deficiency of endothelial Kindlin-2 demonstrates that Notch1 pathway plays a major role in response to Kindlin-2. Paradoxically, VEGFA activates the Notch1 pathway to set up a negative regulatory loop to sustain the permanent angiogenesis [59], and the involvement of elevated Kindlin-2 is revealed in this study.

To ascertain whether the mouse phenotype caused by Kindlin-2 knockout in our study is mediated by integrin activation, we conducted WB analysis using the 9EG7 and 12G10 antibodies on mouse endothelial cells derived from control and cKO mice (Fig. S3A) and HUVECs (Fig. S3B, C). Additionally, we performed further confirmation through IF staining on tissue sections (Fig. S3D). Both results of WB analyses and IF staining lead to the conclusion that Kindlin-2 alterations in endothelial cells do not affect integrin activation states.

Furthermore, there are indeed many publications showing that Kindlin-2 alterations affect integrin activation states; however, there are also publications proving that Kindlin-2 can control organogenesis and homeostasis through integrin-independent mechanisms [12, 60–62].

Angiogenesis is considered as a double-edged sword. Despite that physiological angiogenesis is essential for organ development and homeostasis, aberrant angiogenesis is closely related to serious complications. Therefore, abnormal vasculature is deemed as the target of effective therapy especially for patients who are not suitable for surgery. Due to probable off-target side effects and drug resistance of anti-VEGF/VEGFR agents, it emphasizes the significance of further studying the molecular mechanisms controlling angiogenesis [63]. Our study demonstrates the vital roles of Kindlin-2/Notch1 signaling in physiological angiogenesis, which is in favor of the normal embryonic development. Importantly, we identify Kindlin-2 as a potential switch for regulating angiogenic balance during physiological or pathological processes.

In summary, we for the first time report the key role of endothelial Kindlin-2 in controlling angiogenesis, and we demonstrate that Kindlin-2 is a potential therapeutic target for treatment of angiogenic diseases, such as retinal angioproliferative disorders. There are still some limitations in our study. Firstly, the effect of enhanced endothelial Kindlin-2 on angiogenesis is not identified in vivo. Secondly, although Kindlin-2 is the key regulator to fine-tune the physiological angiogenesis, the involvement and underlying mechanism of endothelial Kindlin-2 in pathological angiogenesis are not revealed. We plan to carry out these investigations in our future study.

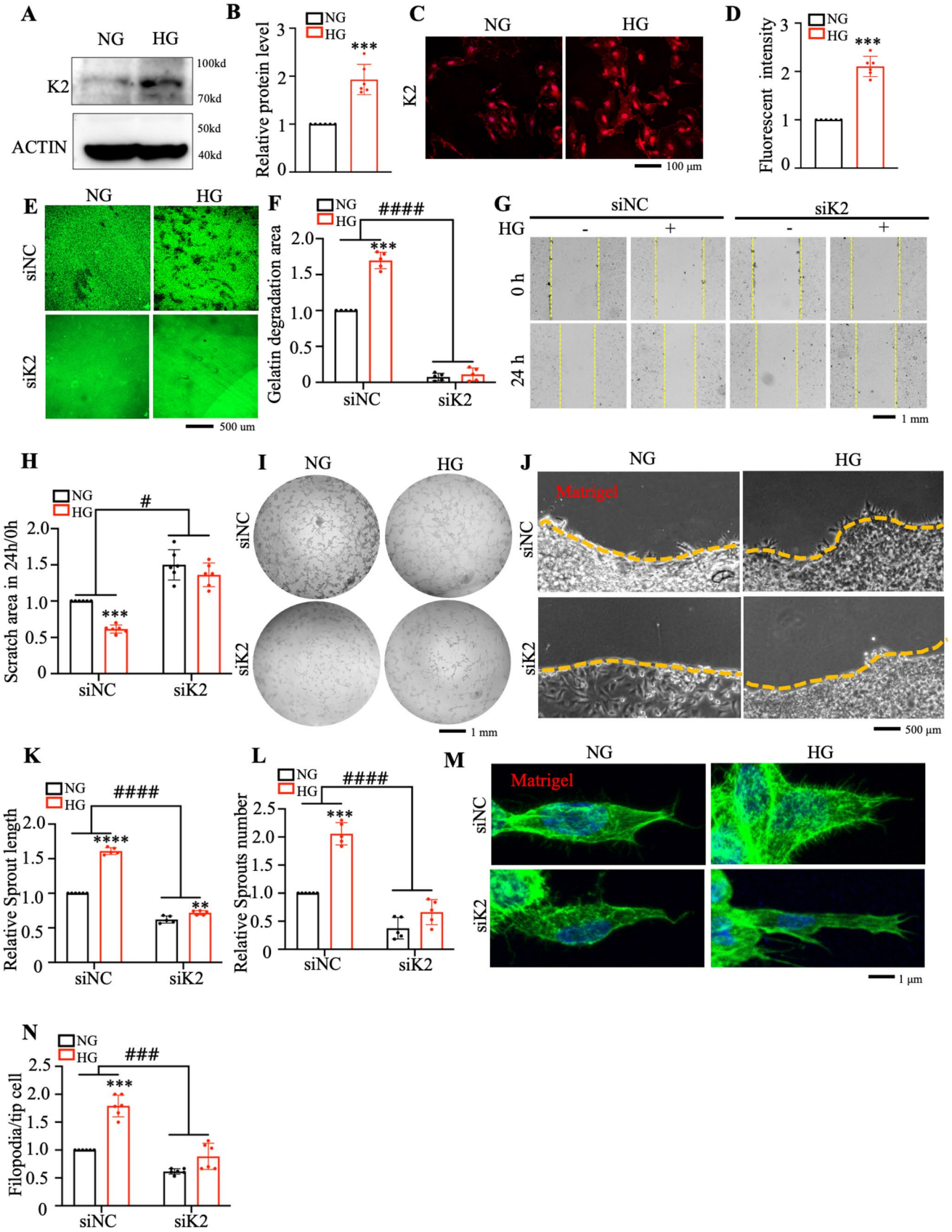
A
NG
HG
K2
ACTIN
100kd
70kd
50kd
40kd
B
NG
HG
Relative protein level
***
C
NG
HG
K2
100 μm
D
NG
HG
Fluorescent intensity
***
E
NG
HG
siNC
siK2
500 um
F
NG
HG
####
***
Gelatin degradation area
siNC
siK2
G
siNC
siK2
HG
0 h
24 h
1 mm
H
NG
HG
#
***
Scratch area in 24h/0h
siNC
siK2
I
NG
HG
siNC
siK2
1 mm
J
NG
HG
Matrigel
siNC
siK2
500 μm
K
NG
HG
####
****
**
Relative Sprout length
siNC
siK2
L
NG
HG
####
***
Relative Sprouts number
siNC
siK2
M
NG
HG
Matrigel
siNC
siK2
1 μm
N
NG
HG
###
***
Filopodia/tip cell
siNC
siK2

◂**Fig. 7** KINDLIN-2 deficiency attenuates the capacity of excessive angiogenesis of HUVECs caused by high glucose (HG). **A, B** Western blotting of KINDLIN-2 ($N=6$ independent experiments, mean ± SD is shown. Student' $t$ test, $^{***}p<0.001$ vs normal glucose). **C**, **D** Immunofluorescence staining of KINDLIN-2 ($N=6$ independent experiments, mean ± SD is shown. Student' $t$ test, $^{***}p<0.001$, vs normal glucose). Scale bars: 100 μm. **E, F** The gelatin degradation assays of HUVECs ($N=5$ independent experiments, mean ± SD is shown. $^{***}p<0.001$, $^{****}p<0.0001$ vs siNC. Two-way ANOVA Bonferroni multiple comparison test, $^{\#\#\#\#}p<0.0001$). Scale bars: 500 μm. **G, H** Representative phase-contrast images of HUVECs taken at 0 h and 24 h after scraping the confluent monolayer cells showed the wound width ($N=6$ independent experiments, mean ± SD is shown. $^{*}p<0.05$, $^{***}p<0.001$, vs siNC. Two-way ANOVA Bonferroni multiple comparison test, $^{\#}p<0.05$). Scale bars: 1 mM. **I** Tube formation ability of HUVECs. $N=5$ independent experiments. Scale bars: 1 mm. **J** Higher magnification images of ECs sprouting into matrigel. Statistics of number (**K**) and length (**L**) of ECs sprouts ($N=5$ independent experiments, mean ± SD is shown, $^{****}p<0.0001$ vs siNC. Two-way ANOVA Bonferroni multiple comparison test, $^{\#\#\#}p<0.001$). Scale bars: 500 μm. **M, N** Higher magnification images of filopodias on activated sprouts. ($N=6$ independent experiments, mean ± SD is shown. $^{***}p<0.001$, $^{****}p<0.0001$ vs siNC. Two-way ANOVA Bonferroni multiple comparison test, $^{\#\#\#}p<0.001$). Scale bars: 1 μm

**Supplementary Information** The online version contains supplementary material available at https://doi.org/10.1007/s00018-023-04866-w.

**Acknowledgements** We thank Prof. Deng Yi, Prof. Ji Shengjian and master student Long Gaoxin of Southern University of Science and Technology (SUSTech) for technical assistance. We acknowledge the assistance of Core Research Facilities of Southern University of Science and Technology.

**Author contributions** YD, GM and HC contributed to study design. YD, GM, XH, YH, ZD, WT, YC and HC contributed to study conducts, data collection and analysis. YD, XH, YH, FR, KL, CD, GM and HC contributed to data interpretation. Drafting the manuscript: YD, HC and GM. DY, GM and HC take the responsibility for the integrity of the data analysis.

**Funding** This work was supported, in part, by the National Key Research and Development Program of China Grants (2019YFA0906001), National Natural Science Foundation of China Grants (82022047 and 81972100), Guangdong Provincial Science and Technology Innovation Council Grant (2017B030301018).

**Data availability** All data of this study are available within the article or the supplementary materials. All data are available from the corresponding authors upon reasonable request.

## Declarations

**Conflict of interest** The authors declare that they have no competing financial interests.

**Ethical approval and consent to participate** There are no human samples used in this study.

**Consent for publication** All authors have agreed for publication.

## References

1. Ma Q, Reiter RJ, Chen Y (2020) Role of melatonin in controlling angiogenesis under physiological and pathological conditions. Angiogenesis 23(2):91–104
2. Liu Z, Tang W, Liu J, Han Y, Yan Q, Dong Y, Liu X, Yang D, Ma G, Cao H (2023) A novel sprayable thermosensitive hydrogel coupled with zinc modified metformin promotes the healing of skin wound. Bioact Mater 20:610–626
3. Yuan W, Wang X (2021) Propranolol participates in the treatment of infantile hemangioma by inhibiting HUVECs proliferation, migration, invasion, and tube formation. Biomed Res Int 2021:6636891
4. Pitulescu ME, Schmidt I, Giaimo BD, Antoine T, Berkenfeld F, Ferrante F, Park H, Ehling M, Biljes D, Rocha SF et al (2017) Dll4 and Notch signalling couples sprouting angiogenesis and artery formation. Nat Cell Biol 19(8):915–927
5. Nagy JA, Benjamin L, Zeng H, Dvorak AM, Dvorak HF (2008) Vascular permeability, vascular hyperpermeability and angiogenesis. Angiogenesis 11(2):109–119
6. Dong Y, Alonso F, Jahjah T, Fremaux I, Grosset CF, Genot E (2022) miR-155 regulates physiological angiogenesis but an miR-155-rich microenvironment disrupts the process by promoting unproductive endothelial sprouting. Cell Mol Life Sci 79(4):208
7. Cao H, Yan Q, Wang D, Lai Y, Zhou B, Zhang Q, Jin W, Lin S, Lei Y, Ma L et al (2020) Focal adhesion protein Kindlin-2 regulates bone homeostasis in mice. Bone Res 2(8):2
8. Chen S, Wu X, Lai Y, Chen D, Bai X, Liu S, Wu Y, Chen M, Lai Y, Cao H et al (2022) Kindlin-2 inhibits Nlrp3 inflammasome activation in nucleus pulposus to maintain homeostasis of the intervertebral disc. Bone Res 10(1):5
9. Fu X, Zhou B, Yan Q, Tao C, Qin L, Wu X, Lin S, Chen S, Lai Y, Zou X et al (2020) Kindlin-2 regulates skeletal homeostasis by modulating PTH1R in mice. Signal Transduct Target Ther 5(1):297
10. Wu C, Jiao H, Lai Y, Zheng W, Chen K, Qu H, Deng W, Song P, Zhu K, Cao H et al (2015) Kindlin-2 controls TGF-beta signalling and Sox9 expression to regulate chondrogenesis. Nat Commun 6:7531
11. Gao H, Zhou L, Zhong Y, Ding Z, Lin S, Hou X, Zhou X, Shao J, Yang F, Zou X et al (2022) Kindlin-2 haploinsufficiency protects against fatty liver by targeting Foxo1 in mice. Nat Commun 13(1):1025
12. Zhu K, Lai Y, Cao H, Bai X, Liu C, Yan Q, Ma L, Chen D, Kanaporis G, Wang J et al (2020) Kindlin-2 modulates MafA and β-catenin expression to regulate β-cell function and mass in mice. Nat Commun 11(1):484
13. Gao H, Guo Y, Yan Q, Yang W, Li R, Lin S, Bai X, Liu C, Chen D, Cao H et al (2019) Lipoatrophy and metabolic disturbance in mice with adipose-specific deletion of kindlin-2. JCI Insight 4(13):e128405
14. He X, Song J, Cai Z, Chi X, Wang Z, Yang D, Xie S, Zhou J, Fu Y, Li W et al (2020) Kindlin-2 deficiency induces fatal intestinal obstruction in mice. Theranostics 10(14):6182–6200
15. Liao Z, Kato H, Pandey M, Cantor JM, Ablooglu AJ, Ginsberg MH, Shattil SJ (2015) Interaction of kindlin-2 with integrin beta3 promotes outside-in signaling responses by the alphaVbeta3 vitronectin receptor. Blood 125(12):1995–2004
16. Pluskota E, Dowling JJ, Gordon N, Golden JA, Szpak D, West XZ, Nestor C, Ma YQ, Bialkowska K, Byzova T et al (2011) The integrin coactivator kindlin-2 plays a critical role in angiogenesis in mice and zebrafish. Blood 117(18):4978–4987
17. Ying J, Luan W, Lu L, Zhang S, Qi F (2018) Knockdown of the KINDLIN-2 gene and reduced expression of Kindlin-2 affects

vascular permeability in angiogenesis in a mouse model of wound healing. Med Sci Monit 24:5376–5383
18. Wei CY, Zhu MX, Zhang PF, Yang X, Wang L, Ying JH, Luan WJ, Chen C, Liu JQ, Zhu M et al (2019) Elevated kindlin-2 promotes tumour progression and angiogenesis through the mTOR/VEGFA pathway in melanoma. Aging (Albany NY) 11(16):6273–6285
19. Pluskota E, Ma Y, Bledzka KM, Bialkowska K, Soloviev DA, Szpak D, Podrez EA, Fox PL, Hazen SL, Dowling JJ et al (2013) Kindlin-2 regulates hemostasis by controlling endothelial cell-surface expression of ADP/AMP catabolic enzymes via a clathrin-dependent mechanism. Blood 122(14):2491–2499
20. Dong Z, Huo J, Liang A, Chen J, Chen G, Liu D (2021) Gamma-Secretase Inhibitor (DAPT), a potential therapeutic target drug, caused neurotoxicity in planarian regeneration by inhibiting Notch signaling pathway. Sci Total Environ 781:146735
21. Kisanuki YY, Hammer RE, Miyazaki J, Williams SC, Richardson JA, Yanagisawa M (2001) Tie2-Cre transgenic mice: a new model for endothelial cell-lineage analysis in vivo. Dev Biol 230(2):230–242
22. Shea K, Geijsen N (2007) Dissection of 6.5 dpc mouse embryos. J Vis Exp 2:160
23. Lin J, Shi Y, Miao J, Wu Y, Lin H, Wu J, Zeng W, Qi F, Liu C, Wang X et al (2019) Gastrodin alleviates oxidative stress-induced apoptosis and cellular dysfunction in human umbilical vein endothelial cells via the nuclear factor-erythroid 2-related factor 2/heme oxygenase-1 pathway and accelerates wound healing in vivo. Front Pharmacol 10:1273
24. Fortini F, Vieceli Dalla Sega F, Caliceti C, Aquila G, Pannella M, Pannuti A, Miele L, Ferrari R, Rizzo P (2017) Estrogen receptor beta-dependent Notch1 activation protects vascular endothelium against tumor necrosis factor alpha (TNFalpha)-induced apoptosis. J Biol Chem 292(44):18178–18191
25. Hsu KS, Guan BJ, Cheng X, Guan D, Lam M, Hatzoglou M, Kao HY (2016) Translational control of PML contributes to TNFalpha-induced apoptosis of MCF7 breast cancer cells and decreased angiogenesis in HUVECs. Cell Death Differ 23(3):469–483
26. Howe GA, Kazda K, Addison CL (2017) MicroRNA-30b controls endothelial cell capillary morphogenesis through regulation of transforming growth factor beta 2. PLoS ONE 12(10):e0185619
27. Diaz B (2013) Invadopodia detection and gelatin degradation assay. Bio Protoc 3(24):e997
28. Wang Z, Zhou L, Wang Y, Peng Q, Li H, Zhang X, Su Z, Song J, Sun Q, Sayed S et al (2021) The CK1delta/epsilon-AES axis regulates tumorigenesis and metastasis in colorectal cancer. Theranostics 11(9):4421–4435
29. Lenter M, Uhlig H, Hamann A, Jenö P, Imhof B, Vestweber D (1993) A monoclonal antibody against an activation epitope on mouse integrin chain beta 1 blocks adhesion of lymphocytes to the endothelial integrin alpha 6 beta 1. Proc Natl Acad Sci USA 90(19):9051–9055
30. Gombash Lampe SE, Kaspar BK, Foust KD (2014) Intravenous injections in neonatal mice. J Vis Exp 93:e52037
31. Hu J, Popp R, Fromel T, Ehling M, Awwad K, Adams RH, Hammes HP, Fleming I (2014) Muller glia cells regulate Notch signaling and retinal angiogenesis via the generation of 19,20-dihydroxydocosapentaenoic acid. J Exp Med 211(2):281–295
32. Zhu M, Jiang L, Yuan Y, Chen L, Liu X, Liang J, Zhu Q, Ding D, Song E (2019) Intravitreal Ets1 siRNA alleviates choroidal neovascularization in a mouse model of age-related macular degeneration. Cell Tissue Res 376(3):341–351
33. Aggarwal BB, Gupta SC, Kim JH (2012) Historical perspectives on tumor necrosis factor and its superfamily: 25 years later, a golden journey. Blood 119(3):651–665
34. Wang Y, Xu J, Zhang X, Wang C, Huang Y, Dai K, Zhang X (2017) TNF-alpha-induced LRG1 promotes angiogenesis and mesenchymal stem cell migration in the subchondral bone during osteoarthritis. Cell Death Dis 8(3):e2715
35. Fu X, Zhou B, Yan Q, Tao C, Qin L, Wu X, Lin S, Chen S, Lai Y, Zou X et al (2020) Kindlin-2 regulates skeletal homeostasis by modulating PTH1R in mice. Signal Transduct Target Ther 5(1):297
36. Teichert M, Milde L, Holm A, Stanicek L, Gengenbacher N, Savant S, Ruckdeschel T, Hasanov Z, Srivastava K, Hu J et al (2017) Pericyte-expressed Tie2 controls angiogenesis and vessel maturation. Nat Commun 8:16106
37. Payne LB, Tewari BP, Dunkenberger L, Bond S, Savelli A, Darden J, Zhao H, Willi C, Kanodia R, Gude R et al (2022) Pericyte progenitor coupling to the emerging endothelium during vasculogenesis via connexin 43. Arterioscler Thromb Vasc Biol 42(4):e96–e114
38. Dehghan M, Narimani N (2020) The element-free Galerkin method based on moving least squares and moving Kriging approximations for solving two-dimensional tumor-induced angiogenesis model. Eng Comput 36(4):1517–1537
39. Barrow-McGee R, Kishi N, Joffre C, Menard L, Hervieu A, Bakhouche BA, Noval AJ, Mai A, Guzman C, Robbez-Masson L et al (2016) Beta 1-integrin-c-Met cooperation reveals an inside-in survival signalling on autophagy-related endomembranes. Nat Commun 7:11942
40. Arjonen A, Alanko J, Veltel S, Ivaska J (2012) Distinct recycling of active and inactive beta1 integrins. Traffic 13(4):610–625
41. Thodeti CK, Matthews B, Ravi A, Mammoto A, Ghosh K, Bracha AL, Ingber DE (2009) TRPV4 channels mediate cyclic strain-induced endothelial cell reorientation through integrin-to-integrin signaling. Circ Res 104(9):1123–1130
42. Tian Y, Xu Y, Fu Q, Chang M, Wang Y, Shang X, Wan C, Marymont JV, Dong Y (2015) Notch inhibits chondrogenic differentiation of mesenchymal progenitor cells by targeting Twist1. Mol Cell Endocrinol 403:30–38
43. Hsu KW, Hsieh RH, Huang KH, Fen-Yau Li A, Chi CW, Wang TY, Tseng MJ, Wu KJ, Yeh TS (2012) Activation of the Notch1/STAT3/Twist signaling axis promotes gastric cancer progression. Carcinogenesis 33(8):1459–1467
44. Anant S, Roy S, VijayRaghavan K (1998) Twist and Notch negatively regulate adult muscle differentiation in Drosophila. Development 125(8):1361–1369
45. Li L, Liu Q, Shang T, Song W, Xu D, Allen TD, Wang X, Jeong J, Lobe CG, Liu J (2021) Aberrant activation of notch1 signaling in glomerular endothelium induces albuminuria. Circ Res 128(5):602–618
46. Jarrett SM, Seegar TCM, Andrews M, Adelmant G, Marto JA, Aster JC, Blacklow SC (2019) Extension of the Notch intracellular domain ankyrin repeat stack by NRARP promotes feedback inhibition of Notch signaling. Sci Signal 12(606):easy2369
47. Ramasamy SK, Kusumbe AP, Wang L, Adams RH (2014) Endothelial Notch activity promotes angiogenesis and osteogenesis in bone. Nature 507(7492):376–380
48. Thurston G, Kitajewski J (2008) VEGF and Delta-Notch: interacting signalling pathways in tumour angiogenesis. Br J Cancer 99(8):1204–1209
49. Nakagawa T, Kosugi T, Haneda M, Rivard CJ, Long DA (2009) Abnormal angiogenesis in diabetic nephropathy. Diabetes 58(7):1471–1478
50. Pedrosa AR, Trindade A, Fernandes AC, Carvalho C, Gigante J, Tavares AT, Dieguez-Hurtado R, Yagita H, Adams RH, Duarte A (2015) Endothelial Jagged1 antagonizes Dll4 regulation of endothelial branching and promotes vascular maturation downstream of Dll4/Notch1. Arterioscler Thromb Vasc Biol 35(5):1134–1146
51. Ai X, Jia Z, Liu S, Wang J, Zhang X (2014) Notch-1 regulates proliferation and differentiation of human bladder cancer cell

lines by inhibiting expression of Kruppel-like factor 4. Oncol Rep 32(4):1459–1464
52. Li D, Xu D, Zhang Y, Chen P, Xie J (2022) Effect of Notch1 signaling on cellular proliferation and apoptosis in human laryngeal carcinoma. World J Surg Oncol 20(1):262
53. Ubezio B, Blanco RA, Geudens I, Stanchi F, Mathivet T, Jones ML, Ragab A, Bentley K, Gerhardt H (2016) Synchronization of endothelial Dll4-Notch dynamics switch blood vessels from branching to expansion. Elife 5:e12167
54. Zhang Z, Wang S, Liu C, Xie R, Hu W, Zhou P (2022) All-in-one two-dimensional retinomorphic hardware device for motion detection and recognition. Nat Nanotechnol 17(1):27–32
55. Stahl A, Connor KM, Sapieha P, Chen J, Dennison RJ, Krah NM, Seaward MR, Willett KL, Aderman CM, Guerin KI et al (2010) The mouse retina as an angiogenesis model. Investig Ophthalmol Vis Sci 51(6):2813–2826
56. Patan S (2004) Vasculogenesis and angiogenesis. Cancer Treat Res 117:3–32
57. Drake CJ, Fleming PA (2000) Vasculogenesis in the day 6.5 to 9.5 mouse embryo. Blood 95(5):1671–1679
58. Prior BM, Yang HT, Terjung RL (2004) What makes vessels grow with exercise training? J Appl Physiol (1985) 97(3):1119–1128
59. Moya IM, Umans L, Maas E, Pereira PN, Beets K, Francis A, Sents W, Robertson EJ, Mummery CL, Huylebroeck D et al (2012) Stalk cell phenotype depends on integration of Notch and Smad1/5 signaling cascades. Dev Cell 22(3):501–514
60. Guo L, Cui C, Zhang K, Wang J, Wang Y, Lu Y, Chen K, Yuan J, Xiao G, Tang B et al (2019) Kindlin-2 links mechano-environment to proline synthesis and tumor growth. Nat Commun 10(1):845
61. Wei X, Xia Y, Li F, Tang Y, Nie J, Liu Y, Zhou Z, Zhang H, Hou FF (2013) Kindlin-2 mediates activation of TGF-β/Smad signaling and renal fibrosis. J Am Soc Nephrol 24(9):1387–1398
62. Guo B, Gao J, Zhan J, Zhang H (2015) Kindlin-2 interacts with and stabilizes EGFR and is required for EGF-induced breast cancer cell migration. Cancer Lett 361(2):271–281
63. Fallah A, Sadeghinia A, Kahroba H, Samadi A, Heidari HR, Bradaran B, Zeinali S, Molavi O (2019) Therapeutic targeting of angiogenesis molecular pathways in angiogenesis-dependent diseases. Biomed Pharmacother 110:775–785